University of Bath

Alternative formats
If you require this document in an alternative format, please contact:
openaccess@bath.ac.uk

18th October 2018

Polymer of Intrinsic Microporosity (PIM-7) Coating Affects Triphasic Palladium Electrocatalysis

Ankita Mahajan [1,2], Prof. Swapan Kumar Bhattacharya [2], Dr. Sébastien Rochat [1], Prof. Andrew D. Burrows [1], Dr. Philip J. Fletcher [3], Dr. Yuanyang Rong [4], Prof. Alan B. Dalton [4], Prof. Neil B. McKeown [5], Prof. Frank Marken*[1]

[1] *Department of Chemistry, University of Bath, Claverton Down, BA2 7AY, UK*

[2] *Physical Chemistry Section, Department of Chemistry, Jadavpur University, Kolkata, 700032, India*

[3] *Materials and Chemical Characterisation Facility (MC^2), University of Bath, Claverton Down, BA2 7AY, UK*

[4] *School of Physics and Astronomy, University of Sussex, Brighton, BN1 9RH, UK*

[5] *School of Chemistry, University of Edinburgh, Joseph Black Building, West Mains Road, Edinburgh, Scotland EH9 3JJ, UK*

Abstract

A film of the polymer of intrinsic microporosity PIM-7 is coated onto a glassy carbon electrode and the resulting effects on electron transfer reactions are studied for three different types of processes: (i) aqueous solution based, (ii) solid state surface immobilised, and (iii) electrocatalytic processes on electrodeposited palladium. The effects on reactivity for hydroquinone oxidation in aqueous phosphate buffer are shown to be linked to microporosity causing a slightly lower rate of mass transport without detrimental effects on electron transfer and reaction kinetics. Next, water-insoluble microcrystalline anthraquinone is immobilised directly into the PIM-7 film and shown to give a chemically reversible reduction process, which is enhanced in the presence of PIM-7, when compared to the case of anthraquinone immobilised directly onto bare glassy carbon. Electrodeposition of a film of nano-palladium is demonstrated to give catalytically active electrodes for the reduction/oxidation of protons/hydrogen, the reduction of oxygen, and for the oxidation of formic acid and methanol. With the PIM-7 film applied onto palladium, a mechanical stabilisation effect occurs. In addition, both the hydrogen insertion and the hydrogen evolution reactions as well as formic acid oxidation are enhanced. Effects are discussed in terms of PIM-7 beneficially affecting the interfacial reaction under triphasic conditions. The microporous polymer acts as an interfacial "gas management" layer.
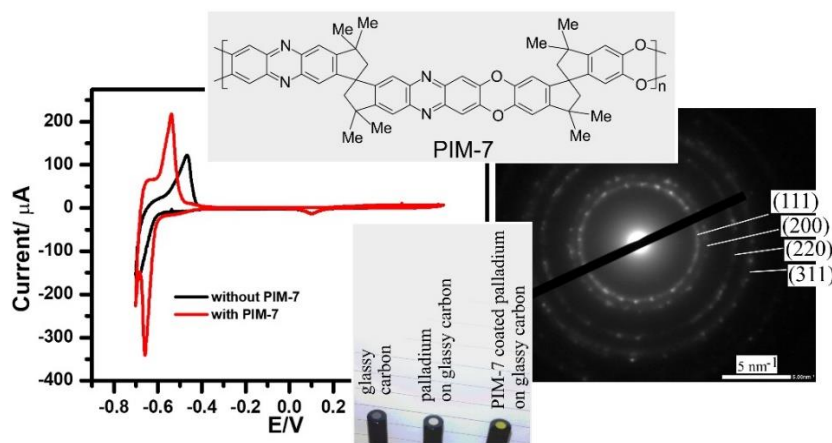
Graphical Abstract:

Graphical Abstract Text: Triphasic electrochemical processes involving gas evolution are beneficially affected by the presence of microporous PIM-7 polymer coated over the electrode surface.

Keywords: palladium; membrane; porosity; selectivity; voltammetry; fuel cell.

2

1. Introduction

In electro-organic synthesis, modified electrodes offer experimental tools for immobilisation of catalysts,[1] induction of chirality,[2] or improved selectivity and enhanced catalytic reactivity.[3,4] In particular microporous films have been developed and coated onto electrodes to aid electrochemical processes based on zeolites,[5] ceramic hybrids,[6] metal-organic frameworks,[7] porous organic cages,[8] and a wide range of polymers.[9] Polymers of intrinsic microporosity (PIMs) represent a relatively new class of synthetic polymers[10] developed recently based on highly rigid polymeric structures to provide rigid 1-2 nm diameter nanopore channel systems with applications in gas separation,[11] gas storage,[12] and electrochemistry.[13] Relevant for applications in electro-organic synthesis are the use of PIMs, for example, to immobilise molecular catalysts[14] and to provide a protective film over nano-metal catalysts.[15,16] The polymer of intrinsic microporosity PIM-1 (see molecular structure in Figure 1) has recently been shown to bind gases such as molecular hydrogen or oxygen at the electrode surface under "triphasic" conditions (with coexisting solid, liquid, and gaseous phases), thereby affecting electrocatalytic reactions.[17] It is of interest to further explore effects of similar PIM coatings on catalytic surfaces.

One considerable advantage of PIMs over other types of microporous materials is their high degree of processability. The polymeric structures of these materials are highly rigid and contorted and the chains are therefore unable to efficiently pack into dense solids (see Figure 1). This leads to low molecular interaction energies in the solid state, highly microporous structures, and good solubility in solvents such as chloroform and cyclopentanone (employed here). As a result, microporous films of PIMs are readily coated over the surface of electrodes or catalysts by solvent evaporation under ambient conditions.

Various types of polymers of intrinsic microporosity have been developed over the recent years,[18] mostly in order to improve gas separation[19] and membrane selectivity.[20] In particular materials such as PIM-1 and PIM-7 (see Figure 1 [21]) have been highlighted for unusual gas separation properties that originate from highly contorted microporous molecular structures. The reported properties of PIM-7 include an average pore radius of 0.48 nm and an average pore volume of 0.47

nm^3,[22] as well as an average molecular weight of $M_w = 51\,000$ g mol^{-1} and a Brunauer-Emmett-Teller (BET) surface area of typically 680 m^2 g^{-1}. The total pore volume was reported as 0.56 cm^3 g^{-1},[23] which suggests a porous channel system with 10^{21} pores per gram. Computational simulation tools have been employed to rationalise the mechanism and rate of gas permeation.[24] Materials such as PIM-7 have been shown to be compatible with roll-to-roll industrial production.[25] So far, there has been no assessment of reactivity of PIM-7 in electrochemical applications.
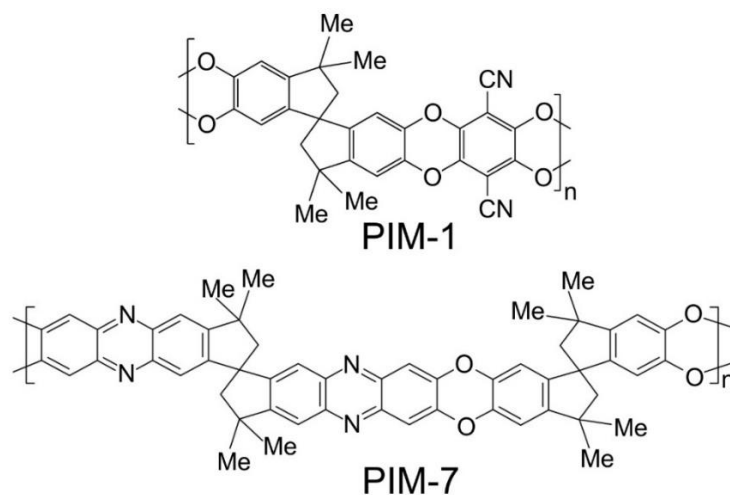
Figure 1. Polymeric structures of PIM-1 and PIM-7

Although primarily developed for applications in gas storage and separation, it has been shown that the intrinsic microporosity and excellent processability of PIMs also lead to new applications in water treatment[26] and in electrochemistry.[27] In this report the effects of PIM-7 on electrochemical processes are studied at modified electrodes immersed in aqueous media. Exploratory experiments are reported for three types of electrode reactions: (i) solution phase redox processes with permeation through the PIM-7 film, (ii) an immobilised solid-state redox system embedded into the microporous PIM-7 film, and (iii) electrocatalysis at nano-palladium electrodeposited onto a glassy carbon substrate and protected by a film of PIM-7. It is suggested that PIM-7 may be considered as an electrochemically inactive (under conditions employed here) microporous film that affects electrode processes by controlling interfacial access and mass transport. There are enhancing effects on electro-organic and on electrocatalytic processes at

palladium involving gaseous hydrogen probably due to PIM-7 affecting the conditions close to the double layer region (*i.e.* wetting of the catalyst surface in competition to gas bubble formation). It is suggested that a film of PIM-7 can be employed to modify and enhance reactivity for some types of electro-organic reactions.

2. Experimental

2.1. Chemical Reagents

Hydroquinone (99%), anthraquinone (97%), palladium(II) chloride ($\geq$ 99.9%), cyclopentanone ($\geq$ 99%), sodium dihydrogen orthophosphate, sodium hydroxide, isopropanol, methanol, 1-butanol (98%), and sulfuric acid (conc. 98%) were purchased from Sigma-Aldrich and used without further purification. PIM-7 was prepared and purified following a previously reported method.[28] Laboratory grade argon gas was obtained from BOC, UK. Solutions were prepared with deionised and filtered water with resistivity of 18.2 MΩ cm (at 22 +/- 2 $^{\circ}$C).

2.2. Instrumentation

Electrochemical measurements were conducted using a potentiostat system (μAUTOLAB III, Metrohm, Herisau, Switzerland) with a K_2SO_4 saturated Hg/Hg_2SO_4 reference electrode (REF621, Radiometer Analytical, with a potential 0.414 V vs. SCE), a 3 mm diameter glassy carbon working electrode (BASi, UK), and a platinum wire counter electrode in a three-electrode custom glass cell. Morphologies of the nano-palladium and palladium with PIM-7 coating were obtained with a JEOL JSM-2010Plus (JEOL U.K. Ltd, Welwyn Garden City, U.K.) high-resolution transmission electron microscope (HR-TEM) using C300Ni100 carbon film 300 mesh nickel TEM grids (EM Resolutions, Sheffield U.K.).

2.3. Procedures

A glassy carbon electrode was coated with a 5 μL volume PIM-7 solution (1 mg PIM-7 mL^{-1} in cyclopentanone) in a drop-cast process followed by drying under ambient conditions. For the

oxidation of hydroquinone (2 mM hydroquinone in 0.1 M phosphate buffer, pH = 7), glassy carbon electrodes without PIM-7 and with PIM-7 were used as the working electrode. For the study of anthraquinone immobilised onto the electrode surface, a glassy carbon without PIM-7 and one coated with 5 µL PIM-7 (1 mg PIM-7 mL^{-1} in cyclopentanone) were initially soaked into 0.1 mM anthraquinone in acetonitrile solution for 20 minutes. The electrodes were then air-dried (to form microcrystalline anthraquinone) and used as working electrode immersed in 0.1 M phosphate buffer (pH = 7).
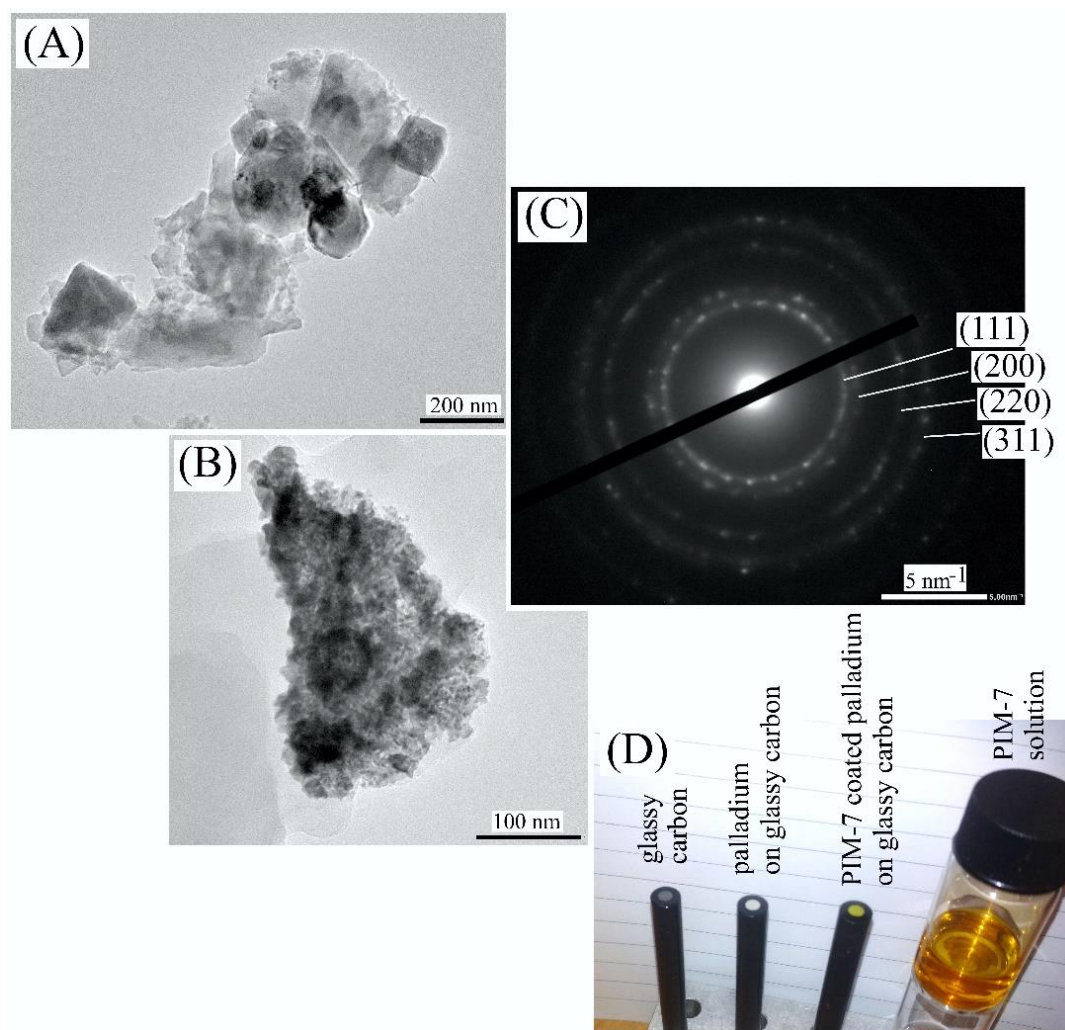
Figure 2. Transmission electron microscopy (TEM) images for nano-palladium dislodged from the glassy carbon electrode (A) as grown and (B) with PIM-7 adhering to the palladium. (C) Electron diffraction data (for the central region in image B) showing the characteristic diffraction lines for palladium. (D) Photographic image of glassy carbon, palladium on glassy carbon, PIM-7 coated palladium on glassy carbon and the PIM-7 solution in cyclopentanone.

For experiments on palladium electrocatalysis, a 1 mM palladium(II) chloride solution was prepared in aqueous 0.1 M HCl solution. Electrodeposition of palladium metal on the glassy carbon was performed in chronoamperometry mode at a deposition potential of –0.5 V vs. Hg/Hg_2SO_4 for a duration of 1000 s (with a charge of approx. 8 mC to give nominally 36 nmol Pd or a weight of 3.8 µg, which translates into a film of approx. 45 nm thickness). Figure 2D shows a photograph of the palladium coating. Electrodes were washed by carefully soaking in deionised water and dried (the palladium coatings were fragile and easily damaged when more vigorously rinsed). If desired, the electrode was then coated with 5 µL solution of PIM-7 (1 mg PIM-7 mL^{-1} in cyclopentanone; giving approx. 0.4 µm thickness) by drop-casting. Measurements were performed either in aqueous 1 M H_2SO_4, 0.1 M formic acid, or in 0.1 M phosphate buffer (pH = 12) solution.

For the preparation of transmission electron microscopy (TEM) grids, a droplet of isopropanol was placed onto the surface of the electrodeposited palladium with/without PIM-7 coating. After gentle scratching with the micropipette tip to dislodge deposit, some of the solution was deposited onto a TEM grid. Figure 2A shows a typical aggregate layer of palladium particles with sizes ranging from 200 nm to much smaller. Figure 2B shows a nano-palladium film still attached to a PIM-7 film. The palladium electron diffraction pattern (Figure 2C) is consistent with that reported previously for nano-palladium.[29]

3. Results and Discussion

3.1. PIM-7 Modified Glassy Carbon I.: Oxidation of Hydroquinone

The effects of PIM-7 film coatings on electrode processes at a glassy carbon electrode surface are first investigated with the hydroquinone redox system in phosphate buffer at pH 7. Figure 3 shows cyclic voltammetry data contrasting the case of no PIM-7 coating (Figure 3A) with that of with PIM-7 coating (Figure 3C). The appearance of both reduction peak (at *ca.* –0.5 V vs. Hg/Hg_2SO_4) and the re-oxidation peak (at *ca.* –0.1 V vs. Hg/Hg_2SO_4) remains very similar without and with

PIM-7 applied to the electrode surface. Only the magnitude of the peak currents is diminished in the presence of the microporous PIM-7 film, presumably due to mass transport limitations in the nanopores of approximately 1-2 nm diameter. The shape of peaks appears broader (tending towards sigmoidal) in the presence of PIM-7 due to onset of thin film diffusion with a mobile but lower hydroquinone concentration in the polymer film.
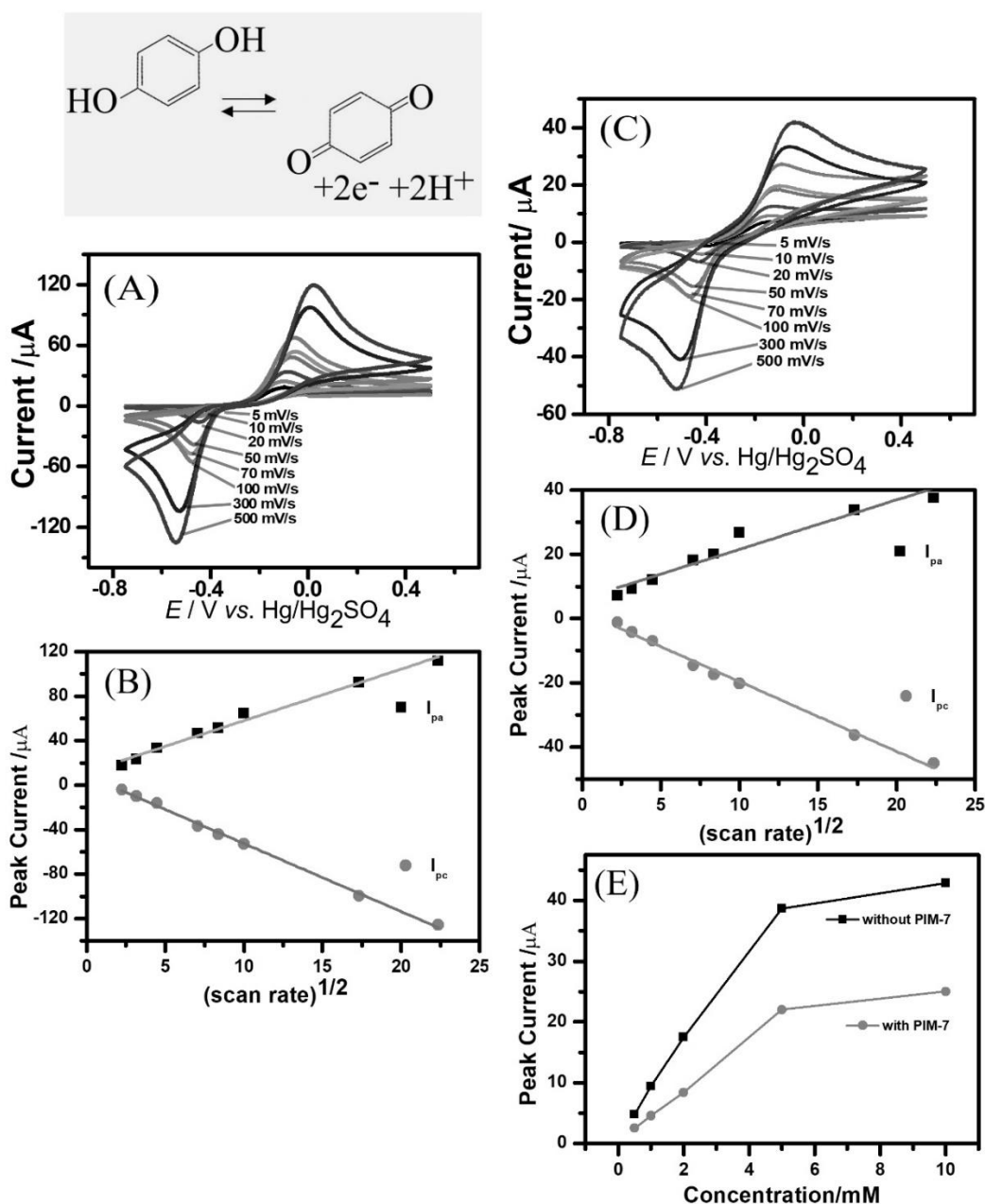
Figure 3. (A) Cyclic voltammograms for the oxidation of 2 mM hydroquinone in 0.1 M phosphate buffer (pH = 7) obtained at a glassy carbon electrode without PIM-7, (B) Plot of peak currents (for oxidation I_{pa} and for reduction I_{pc}) *versus* square root of scan rate. (C) as above with PIM-7 coating.

(D) Plot of peak current *versus* square root of scan rate. (E) Plot of anodic peak current *versus* concentration of hydroquinone obtained at the scan rate of 5 mVs^{-1}.

A plot of peak currents *versus* square root of scan rate is shown for both voltammograms obtained without PIM-7 (Figure 3B) and voltammograms obtained with PIM-7 coated over glassy carbon (Figure 3D). In the absence of PIM-7, peak currents scale reasonably well with the square root of scan rate, indicative of current peaks that are limited by planar diffusion to the electrode surface.[30] In contrast, in the presence of PIM-7 only the low scan rate data seem to scale and at scan rates higher than 100 mVs^{-1} the anodic current peaks seem lower. The shape of the peak changes to more sigmoidal, which could be a sign of the PIM-7 layer restricting mass transport in particular when going to higher scan rates. Both, the apparent concentration of hydroquinone and the apparent diffusion coefficient of hydroquinone are likely to be slightly lowered in the PIM-7 environment, which fully explains the observed behaviour. The shape of voltammograms for hydroquinone oxidation is sensitive to the buffer environment and pH and both of these seem essentially the same in the aqueous solution and within the PIM-7 microporous structure. One would expect more significant effects of the polymer on electron transfer kinetics probably for thicker PIM-7 films and for higher hydroquinone concentrations, and therefore further study will be needed to explore these effects in more depth.

3.2. PIM-7 Modified Glassy Carbon II.: Reduction of Anthraquinone

Next, the immobilisation of a redox-active microcrystalline solid, anthraquinone, first onto bare glassy carbon and then into the PIM-7 film on glassy carbon is investigated as a case of solid state electrochemistry. Microcrystalline deposits of electrically insulating materials at electrode surfaces are known to show electrochemical activity linked to the redox processes at the triple phase boundary[31] and linked to solid state conversions.[32] Anthraquinone is highly water-insoluble, but remains electrochemically redox active when in direct contact to the electrode surface. In previous studies, anthraquinone was shown to undergo a 2-electron 2-proton reduction[33] (see Figure 4), which is sensitive to pH and to ionic strength in solution.[34] Immobilisation of redox active but water-insoluble guest molecules into PIM films at electrode

9

surfaces has been previously reported also for the porphyrin metal complex FeTPP[35] and for TEMPO organocatalysts[36] for the oxidation of alcohols to aldehydes.

In this study, PIM-7 is first deposited from cyclopentanone onto the glassy carbon surface. The electrode is then immersed into 0.1 mM anthraquinone in acetonitrile (PIM-7 is not soluble in acetonitrile) and after drying under ambient conditions some anthraquinone is immobilised onto the electrode surface. Figure 4A shows three consecutively recorded cyclic voltammograms for the reduction of anthraquinone immobilised at a bare glassy carbon electrode. A chemically reversible process is observed with $E_{mid} = \frac{1}{2} (E_{p,ox} + E_{p,red}) = -0.93$ V vs. Hg/Hg$_2$SO$_4$.[37] In the first couple of potential cycles the current diminishes, but then stabilises towards the 10th potential cycle.
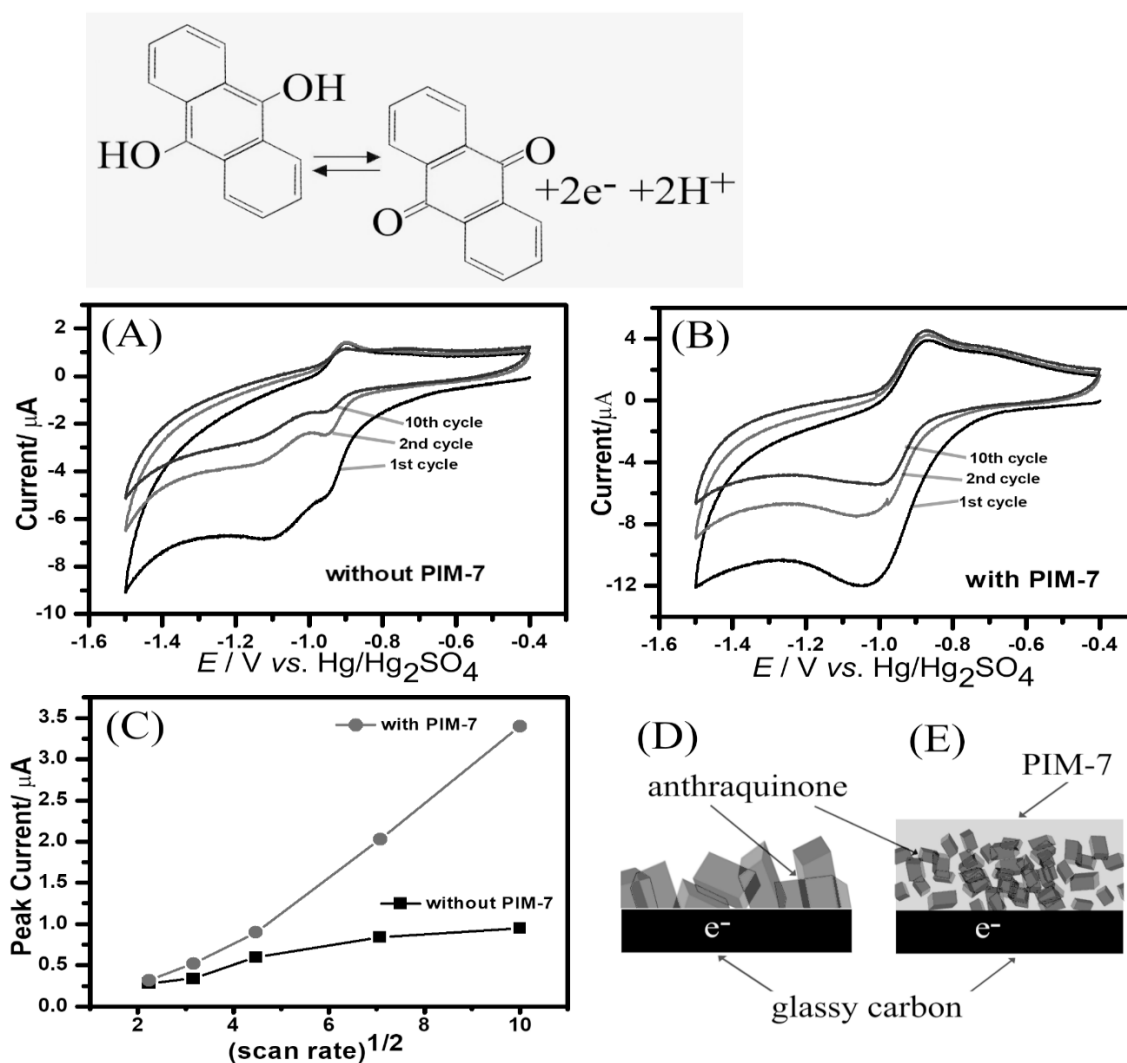
Figure 4. Reaction scheme for the 2-electron 2-proton anthraquinone reduction. Cyclic voltammograms (first, second, and tenth cycles; scan rate 0.1 Vs^{-1}) obtained (A) at a glassy carbon electrode and (B) a PIM-7 film modified glassy carbon electrode (both dipped into the 0.1 mM anthraquinone dissolved in acetonitrile for 20 min and ambiently dried) immersed in 0.1 M phosphate buffer pH 7. (C) Plots of anodic peak currents *versus* square root of scan rate. Schematic drawings (D) and (E) represent conditions at the electrode surface with/without PIM-7.

There are two processes with very similar E_{mid}, one with a peak-to-peak separation of close to 60 mV and a second broader signal with peak-to-peak separation of close to 350 mV (the anodic peak feature at -0.75 V vs. Hg/Hg$_2$SO$_4$ is relatively small compared to the cathodic peak at -1.1 V vs. Hg/Hg$_2$SO$_4$ probably due to transport effects in the solid state or on the solid surface). The former

process could be associated with a surface layer of anthraquinone, whereas the latter may be tentatively assigned to a second layer deeper within the crystal surface. The same experiment performed in the presence of the PIM-7 film on the glassy carbon electrode gives a similar result, although currents are generally higher and the process with smaller peak-to-peak separation is enhanced. This is likely to be linked to the presence of many more and smaller anthraquinone microcrystals within the microporous PIM-7 host structure. The effect could also be linked to the local buffer concentration at the electrode surface with PIM-7 providing additional porosity and thereby better buffer access during anthraquinone reduction. The plot in Figure 4C summarises peak current data in a format similar to that in Figure 3, but it has to be kept in mind that data here is likely to be linked to considerably more complex processes.

The results demonstrate that PIM-7 is readily modified with solid state redox systems. The aqueous solution environment within the PIM-7 coating closely matches that in bulk solution and therefore the mechanism for solid state anthraquinone reduction appears to be retained. This is a useful model case for processes requiring immobilisation of water-insoluble molecular or inorganic electrocatalysts, but more detailed study will be required in future to better reveal the local conditions at the electrode surface during electron transfer within the polymer coating.

3.3. PIM-7 Modified Glassy Carbon III.: Palladium Electrodeposition and Hydrogen Evolution

Next, a film of nano-palladium is electrodeposited onto the glassy carbon electrode surface to be employed as electrocatalyst bare and when stabilised with a PIM-7 film coating. Figure 2D shows a photograph where the presence of the palladium film is revealed as a thin mirror-like reflective layer, which after coating with PIM-7 takes on a slightly orange colouration (compare the colour of the PIM-7 solution). From TEM data (Figure 2) it can be seen that rather non-uniform nano-scale palladium nanoparticles of up to 200 nm size are present in the metal film deposit with *ca.* 45 nm estimated thickness (based on electrolytic charge passed during deposition). In contrast the PIM-7 coating is estimated to be 400 nm thick (*vide supra*).

The presence of the palladium film is confirmed in electrochemical measurements (see Figure 5). In aqueous 1 M H_2SO_4 clear evidence for the presence of palladium is seen (i) in the oxide region from 0.2 V vs. Hg/Hg_2SO_4 to 0.7 V vs. Hg/Hg_2SO_4. Upon reversing the scan direction the palladium oxide is converted back into palladium metal in a well-defined peak at 0.1 V vs. Hg/Hg_2SO_4,[38] which is known to be associated with some more complex reaction steps leading to Pd metal.[39] The charge under this peak can be employed to estimate the palladium surface area (based on a conversion constant of approx. 405 µC cm^{-2} [40]), which is here constant at *ca.* 0.18 cm^2 (see Figure 5A; consistent with a roughness factor 2.5).

The hydrogen region for the palladium coated electrode starts at –0.4 V vs. Hg/Hg_2SO_4. Initially, hydrogen is deposited as a mono-layer onto the palladium surface. In Figure 4B this can be seen in the extended potential window to –0.6 V vs. Hg/Hg_2SO_4, where a double-peak feature is seen. This feature seems close to identical for the bare nano-palladium and for the PIM-7 coated nano-palladium. However, when extending the potential window more negatively, a higher cathodic current is observed and a peak feature is detected. This peak feature occurs at –0.70 V vs. Hg/Hg_2SO_4 for the bare palladium, but is shifted to –0.65 V vs. Hg/Hg_2SO_4 for the PIM-7 coated palladium (Figure 4C). The process can be identified as the binding of hydrogen into the palladium bulk.[41] Perhaps surprisingly, after reversal of the scan direction peaks are again observed at different peak potentials at –0.48 V vs. Hg/Hg_2SO_4 for bare palladium and at –0.52 V vs. Hg/Hg_2SO_4 for the PIM-7 coated palladium. That is, although the midpoint potential for this process remains identical with/without PIM-7, the peak-to-peak separation is affected, This is consistent with the formation of the same product (PdH$_x$ with $0.0 < x < 1.0$ with a phase transformation at $x = 0.7$ [42]) but with a change in rate. For both reduction and oxidation processes the PIM-7 coated nano-palladium reacts faster. Note that the electrochemically active surface area for the two electrodes is not significantly different and therefore this effect seems to originate from the presence of PIM-7 at the interface palladium | aqueous electrolyte as depicted schematically in Figure 5F.
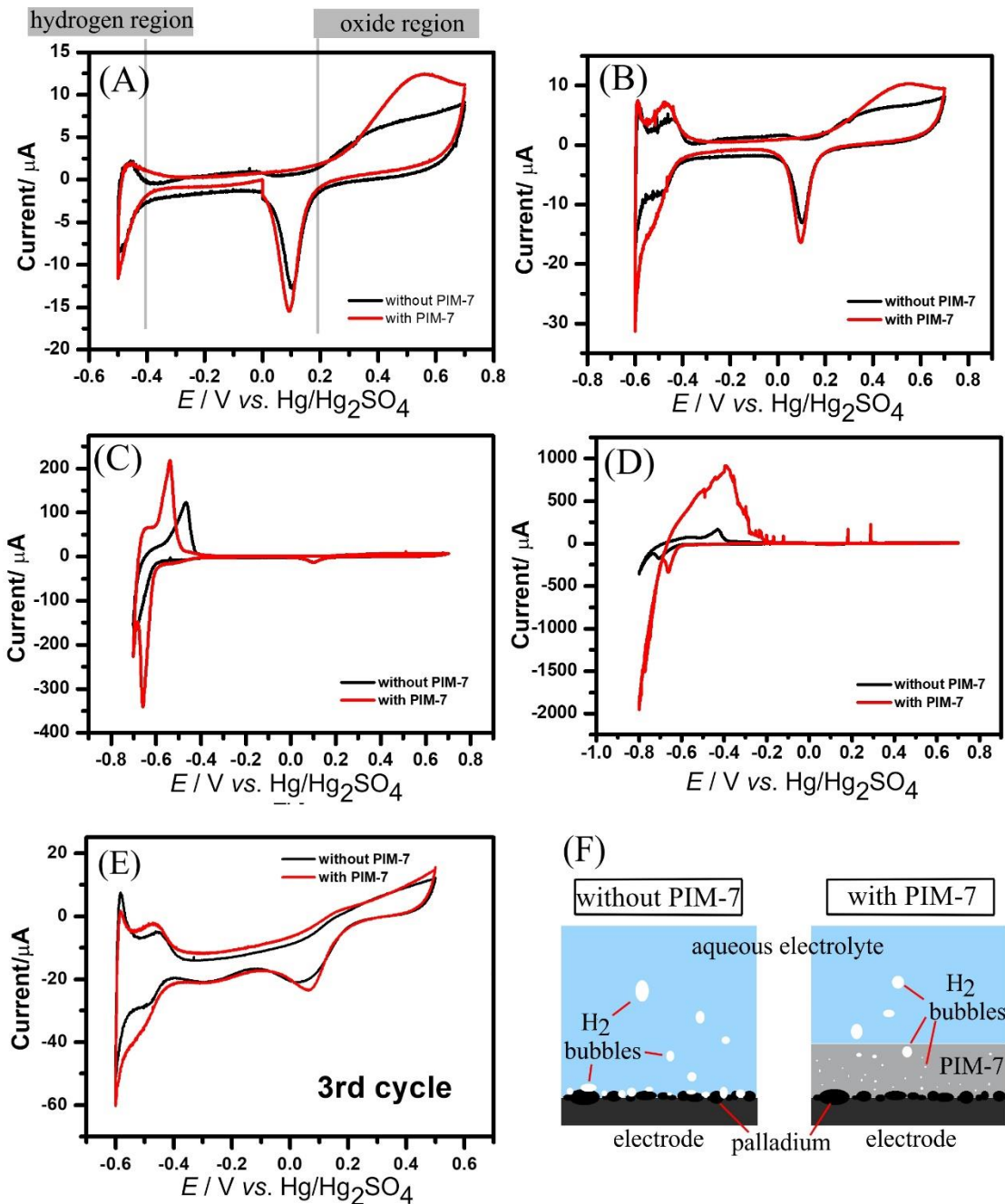
Figure 5. Cyclic voltammograms (in argon-purged solution; scan rate 0.02 Vs^{-1}) for a palladium-coated glassy carbon electrode (black) and for a palladium and PIM-7 coated glassy carbon electrode (red) immersed in aqueous 1 M H$_2$SO$_4$ solution over a potential window (A) 0.7 to –0.5 V vs. Hg/Hg$_2$SO$_4$, (B) 0.7 to –0.6 V vs. Hg/Hg$_2$SO$_4$, (C) 0.7 to –0.7 V vs. Hg/Hg$_2$SO$_4$, and (D) 0.7 to –0.8 V vs. Hg/Hg$_2$SO$_4$. (E) Cyclic voltammogram (in aerated solution, scan rate 0.02 Vs^{-1}) for the reduction of oxygen. (F) Schematic drawing to illustrate the PIM-7 structure interacting as a "gas management" layer with a palladium surface.

When extending the potential window further negative, the hydrogen evolution process is observed. Again, in the presence of PIM-7 on the palladium surface the hydrogen evolution reaction is substantially faster. Also, hydrogen evolved in the presence of PIM-7 is "trapped" and re-oxidised (see the broad peak in Figure 5D) consistent with recent observations of hydrogen storage in PIM-1 materials.[17] The onset of hydrogen evolution is linked to the position of the reduction peak (formation of PdH$_x$) and both processes are likely to be coupled. Therefore, the shift in the peak to more positive potential and the enhanced rate in hydrogen evolution caused by PIM-7 should depend on a similar mechanism. It seems likely that the ability of PIM-7 (similar to PIM-1) to store hydrogen in nanochannels could lead to this type of enhancement. However, alternatively it may also be possible that the PIM-7 in the vicinity of the palladium surface causes a disturbance in the way water and/or hydrogen can interact with the surface (Figure 5F). In this particular case the presence of gas bubbles at the catalyst surface could be detrimental/blocking and the PIM-7 coating could act as a "gas management" layer taking away the bubbles and providing a more active catalyst surface.

Figure 5E is shown in contrast to data in Figure 5B, and it demonstrates the effects of ambient oxygen on the voltammetric responses. At both types of electrode with/without PIM-7 coating, the oxygen reduction process commences at 0.1 V vs. Hg/Hg$_2$SO$_4$. The similarity in the voltammetric features suggests that oxygen readily diffuses into the PIM-7 and it undergoes electrochemical reduction in a similar manner with or without PIM-7. It is interesting to expand this study to other related catalytic processes, in which gas (hydrogen) evolution is involved and PIM-7 effects predicted.

3.4. PIM-7 Modified Glassy Carbon IV.: Palladium Electrodeposition, Formic Acid Oxidation, and Methanol Oxidation

A classic case of a catalytic reaction on palladium catalysts is the oxidation of formic acid. This process is important for example in fuel cell systems[43] based on formic acid as a hydrogen storage fuel.[44] The oxidation of formic acid in acidic aqueous media is known to occur with some complexity in the mechanism.[45] There are three reaction pathways[46,47] for the oxidation of

formic acid on palladium linked to (i) the direct pathway via 2-electron transfer and formation of CO_2, (ii) the indirect pathway via dehydration and formation of CO followed by oxidation, and (iii) the hydrogen pathway based on HCOOH converting to CO_2 and H_2 [48,49] with the latter then being oxidised.[50] Catalytic formic acid decomposition reactions have been proposed based on palladium causing spontaneous formation of hydrogen.[51] It is interesting to explore the effects of PIM-7 on the process based on the hydrogen pathway.

Figure 6A shows cyclic voltammograms for the oxidation of aqueous 0.1 M formic acid at the electrodeposited palladium film on glassy carbon. The equilibrium potential under these conditions is at approximately –0.7 V vs. Hg/Hg_2SO_4 consistent with the potential for hydrogen evolution (compare Figure 5D). The overlay of data for the bare palladium film (black) and the PIM-7 coated palladium film (red) clearly reveals the difference in reactivity. In the presence of PIM-7 oxidation currents are enhanced to approximately twice of those observed in the absence of PIM-7. In addition, the potentials where the formic acid oxidation seizes (on the positive going potential scan entering the oxide region) and re-starts (on the negative going potential scan) are clearly shifted to more positive values. The reason for this shift is currently not fully understood (the local pH or presence/absence of bubbles on the Pd surface may be factors). The localised storage of some hydrogen in the PIM-7 coating could help remove the oxide film and in this way cause the observed pattern.

When increasing the scan rate, the magnitude of current peaks increases (Figure 6) and a hysteresis in forward and backward voltammetric responses occurs. Figure 7 shows data obtained by cyclic voltammetry in aqueous formic acid with a scan rate of 100 mVs^{-1} and as a function of formic acid concentration. It can be observed that significant enhancement effects by the PIM-7 film are apparent particularly at higher concentration of formic acid. Figure 7E shows data for 0.2 M formic acid with almost four-fold increase in currents. A summary of currents is shown in a plot in Figure 7F. The enhancement effect is proposed to be associated with a faster rate and with some degree of hydrogen storage within the PIM-7 film without the formation of bubbles that block the electrode surface. Next, redox processes are investigated that occur without the spontaneous formation of hydrogen.
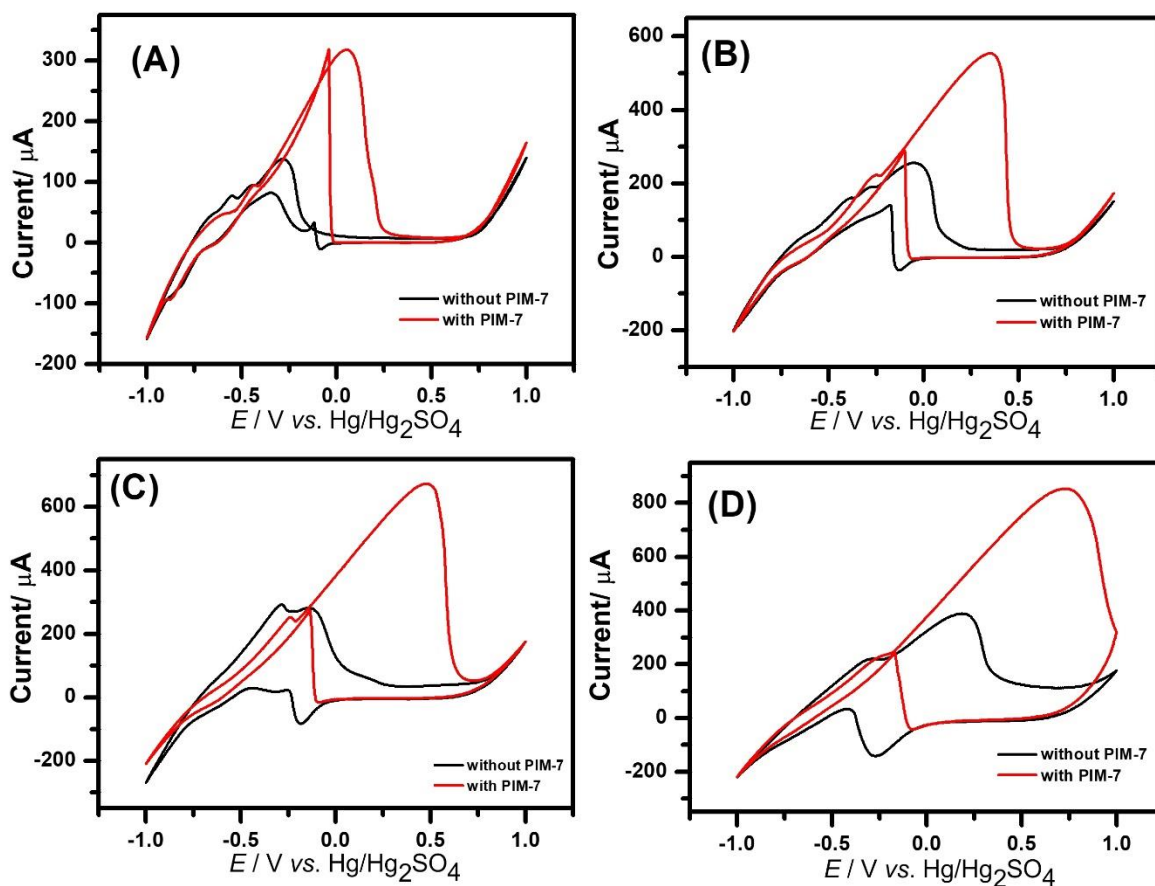
Figure 6. Cyclic voltammograms (scan rate of (A) 10 ms^{-1}, (B) 50 mVs^{-1} , (C) 100 mVs^{-1}, and (D) 500 mVs^{-1}) for a palladium-coated glassy carbon electrode (black) and for a palladium and PIM-7 coated glassy carbon electrode (red) immersed in aqueous 0.1 M formic acid solution.
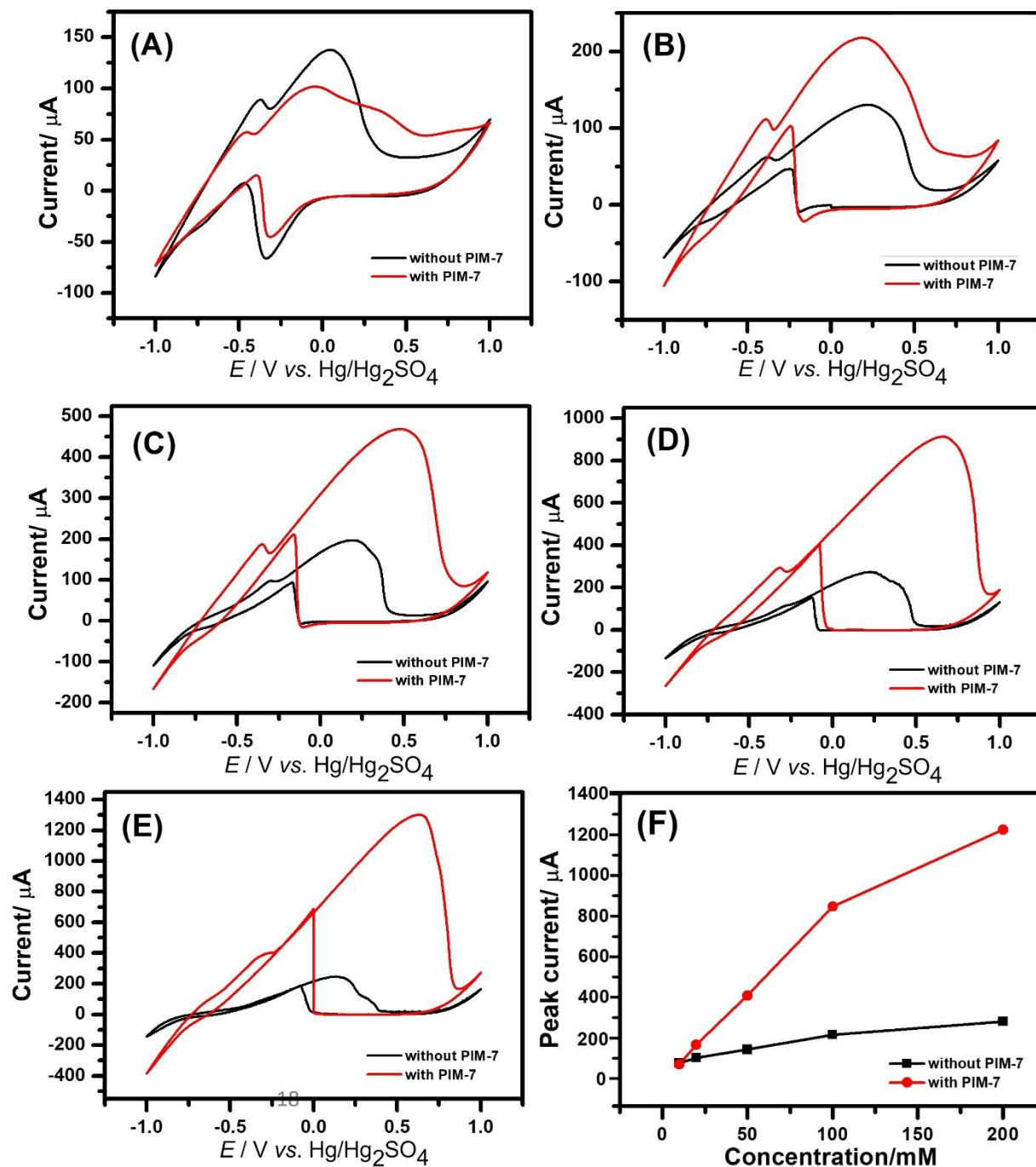
Figure 7. Cyclic voltammograms (scan rate of 100 mVs⁻¹) for a palladium-coated glassy carbon electrode (black) and for a palladium and PIM-7 coated glassy carbon electrode (red) immersed in aqueous (A) 10 mM, (B) 20 mM, (C) 50 mM, (D) 100 mM and (E) 200 mM formic acid solution. (F) Plot of peak currents *versus* concentration of formic acid.

Palladium is well known to catalyse the oxidation of aliphatic alcohols such as methanol,[52,53] ethanol,[54] or butanol.[55] In general, palladium electrocatalysis has been considered for direct alcohol fuel cells[56] as well as for the valorisation of glycerol.[57] Here, the oxidation of methanol is investigated in aqueous 0.1 M phosphate buffer media. This process is sensitive to pH (at pH 7 only insignificant levels of catalytic activity are observed and therefore work here is reported for pH 12) and sensitive to the nature of the alcohol (tests with butanol revealed mechanical instability and detachment of the catalyst layer, and relatively low reactivity for both cases, with or without PIM-7 coating and at pH 12).

Figure 8A shows cyclic voltammetry data for the oxidation of 33 mM methanol in 0.1 M phosphate buffer pH 12 (under argon) for bare palladium (black) and for PIM-7 coated palladium (red). The reduction peak at –0.7 V vs. Hg/Hg_2SO_4 can be attributed to the conversion of oxide to palladium metal. The oxidation peak at approximately –0.5 V vs. Hg/Hg_2SO_4 is associated mainly with the oxidation of methanol. The presence of the PIM-7 coating clearly hinders the methanol oxidation. When increasing the concentration of methanol to 166 mM (Figure 8B) a similar pattern is observed. With a methanol concentration of 1.0 mol dm^{-3} (Figure 8C) a cross-over point seems to have been reached (see also the plot in Figure 8D), but this is not linked to enhanced catalysis. The palladium film coating is mechanically weakly adhered to the glassy carbon substrate and the presence of organic components seem to further weaken the bond. In the plot of peak current *versus* methanol concentration the loss of activity is linked here most likely to the loss of palladium from the electrode surface (and not molecular scale kinetic effects). The PIM-7 coating does prevent the loss of palladium in this case. However, in contrast to observations for formic acid oxidation, there seems to be no significant current enhancement due to the presence of PIM-7. This could be a further indication that indeed gas (hydrogen) evolving reactions benefit most from the coating with microporous PIM-7.
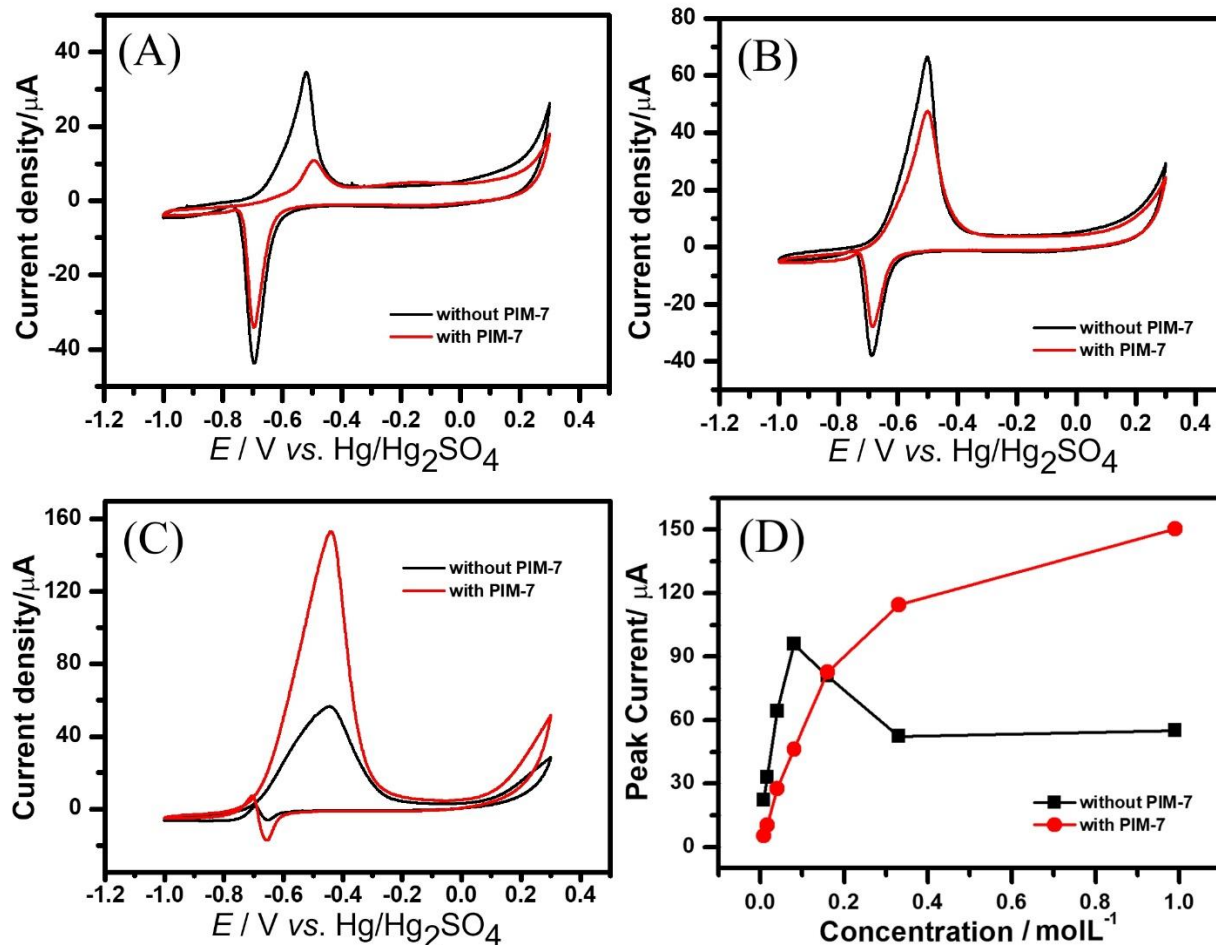
Figure 8. Cyclic voltammograms (scan rate 10 mVs^{-1}) for a palladium-coated glassy carbon electrode (black) and for a palladium and PIM-7 coated glassy carbon electrode (red) in (A) 0.03 mol dm^{-3}, (B) 0.17 mol dm^{-3}, (C) 1.0 mol dm^{-3} methanol in 0.1 M phosphate buffer pH 12. (D) Plot of peak current *versus* concentration (mol dm^{-3}) of methanol. Note that mechanical damage to the Pd catalyst without PIM-7 protection occurs at a methanol concentration of approx. 0.2 mol dm^{-3}.

Further experiments with methanol were performed also in 1 M H$_2$SO$_4$ but instability of the palladium film (without or with PIM-7 coating) prevented meaningful measurements in this system. The presence of organic components in the reaction mixture seems to cause surface tension effects that destabilise the palladium – glassy carbon interface and in this way lead to damage of the catalyst layer. It seems likely that in future better conditions for adhesion can be found with a different rougher carbon substrate or with nano-palladium dispersed in Vulcan carbon[58] to give mechanically stable catalyst systems with PIM protection. However, benefits from the PIM-7

coating in terms of enhanced catalytic kinetics appear to be limited to cases with the presence of gaseous reactants or triphasic reaction conditions. Therefore, future applications of PIM-7 coatings in electro-organic synthesis could be of interest primarily in cases such as CO_2 reduction or for reactions requiring N_2, O_2, CH_4, or ethylene as gaseous reagents interacting with electrocatalytic surfaces.

4. Conclusions

It has been shown that a coating of PIM-7 provides a stable microporous film that allows smaller molecules such as hydroquinone and methanol reactants to diffuse in and reaction products to diffuse out. For water-insoluble species such as anthraquinone, the PIM-7 film offers a host, in which microcrystalline solid material is immobilised close to the electrode surface to undergo redox transformations. When studying electrocatalysis at palladium film coatings, it became apparent that PIM-7 can affect the processes that are linked to the hydrogen evolution reaction. Both, the formation of PdH_x and the formation of hydrogen gas during hydrogen evolution seemed to occur at an enhanced rate, but also the formation (oxidation) of hydrogen from formic acid was enhanced in the presence of the PIM-7 coating. All of these phenomena are suggested to be linked to compositional changes at the palladium | aqueous electrolyte interface due to the presence of the microporous PIM-7 coating. The most likely interpretation of the data appears to be a scenario in which hydrogen gas can be absorbed into the PIM-7 film without interfacial nucleation of hydrogen bubbles and catalyst blocking at the palladium surface. In this way the palladium surface can remain active and processes can occur with an apparently enhanced rate. The PIM-7 coating can act as a "gas management" layer at the interface. In this way PIM coatings could be useful in electrochemical technology to lower overpotentials and to bring down energy costs. This conclusion is consistent with observations for methanol oxidation electrocatalysis, where the effects of PIM-7 on the rate are weak and detrimental rather than beneficial.

In the future, a wider range of PIM materials could be screened and investigated so that gas absorption and permeability under triphasic reaction conditions can be correlated with effects on the rate of electrocatalytic processes. Further work will be required addressing the question of

adhesion between PIM coatings and the underlying electrode. Most beneficial appears to be the PIM-7 induced combination of mechanical stabilisation of nano-catalysts and enhanced reactivity in processes involving gaseous reagents in aqueous media. There are many triphasic electrocatalytic processes (involving O_2, CO_2, H_2, N_2, etc.) where beneficial effects could be possible. Furthermore, PIM-based materials could be combined with metal or carbon nano-materials to provide nano-composite electrodes with enhanced gas diffusion properties, surface area, and reactivity.

Acknowledgements

References

[1]   R. Francke, R.D. Little, *Chem. Soc. Rev.* **2014**, *43*, 2492–2521.

[2]   O. Onomura, *Heterocycles* **2012**, *85*, 2111–2133.

[3]   C. Li, Y. Kawamata, H. Nakamura, J.C. Vantourout, Z.Q. Liu, Q.L. Hou, D.H. Bao, J.T. Starr, J.S. Chen, M. Yan, P.S. Baran, *Angew. Chem. Int. Ed.* **2017**, *56*, 13088–13093.

[4]   J.C. Lo, D. Kim, C.M. Pan, J.T. Edwards, Y. Yabe, J.H. Gui, T. Qin, S. Gutierrez, J. Giacoboni, M.W. Smith, P.L. Holland, P.S. Baran, *J. Am. Chem. Soc.* **2017**, *139*, 2484–2503.

[5]   K.L. Yeung, W. Han, *Catal. Today*, **2014**, *236*, 182–205.

[6]   X.Y. Wu, K.X. Wang, J.S. Chen, *Prog. Chem.* **2012**, *24*, 262–274.

[7]   X.M. Liu, B. Tang, J.L. Long, W. Zhang, X.H. Liu, Z. Mirza, *Sci. Bull.* **2018**, *63*, 502–524.

[8]   N. Hernández-Ibáñez, J.S.M. Lee, J. Iniesta, V.M. Leguey, M.E. Briggs, A.I. Cooper, E. Madrid, F. Marken, *J. Electroanal. Chem.* **2017**, *819*, 46–50.

[9]   A. Malinauskas, *Synth. Metals,* **1999**, *107*, 75–83.

[10]   N.B. McKeown, *Sci. China Chem.* **2017**, *60*, 1023–1032.

[11]   N.B. McKeown, P.M. Budd, *Macromolecules*, **2010**, *43*, 5163–5176.

[12]   C. Xu, N. Hedin, *Mater. Today*, **2014**, *17*, 397–403.

[13]   E. Madrid, N.B. McKeown, *Curr. Opinion Electrochem.* **2018**, *10*, 61–66.

[14]   S.D. Ahn, A. Kolodziej, R. Malpass-Evans, M. Carta, N.B. McKeown, S.D. Bull, A. Buchard, F. Marken, *Electroanalysis*, **2016**, *7*, 70–78.

[15]   D.P. He, Y.Y. Rong, M. Carta, R. Malpass-Evans, N.B. McKeown, F. Marken, *RSC Adv.* **2016**, *6*, 9315–9319.

[16]   Y.Y. Rong, R. Malpass-Evans, M. Carta, N.B. McKeown, G.A. Attard, F. Marken, *Electroanalysis*, **2014**, *26*, 904–909.

[17]   E. Madrid, J. Lowe, K. Msayib, N.B. McKeown, F. Marken, *ChemElectroChem*, **2018**, https://doi.org/10.1002/celc.201800177.

[18]   N.B. McKeown, P.M. Budd, *Chem. Soc. Rev.* **2006**, *35*, 675–683.

[19]   Z.X. Low, P.M. Budd, N.B. McKeown, D.A. Patterson, *Chem. Rev.* **2018**, *118*, 5871–5911.

[20]   C.G. Bezzu, M. Carta, M.C. Ferrari, J.C. Jansen, M. Monteleone, E. Esposito, A. Fuoco, K. Hart, T.P. Liyana-Arachchi, C.M. Colina, N.B. McKeown, *J. Mater. Chem. A*, **2018**, *6*, 10507–10514.

[21]   P.M. Budd, K.J. Msayib, C.E. Tattershall, B.S. Ghanem, K.J. Reynolds, N.B. McKeown, D. Fritsch, *J. Membrane Sci.* **2005**, *251*, 263–269.

[22]   R.L. de Miranda, J. Kruse, K. Ratzke, F. Faupel, D. Fritsch, V. Abetz, P.M. Budd, J.D. Selbie, N.B. McKeown, B.S. Ghanem, *Phys. Status Solidi Rapid Res. Lett*. **2007**, *1*, 190–192.

[23]   B.S. Ghanem, N.B. McKeown, P.M. Budd, D. Fritsch, *Macromolecules*, **2008**, *41*, 1640–1646.

[24]   W.J. Fang, L.L. Zhang, J.W. Jiang, *Mol. Simulation*, **2010**, *36*, 992–1003.

[25]   M. Cook, P.R.J. Gaffney, L.G. Peeva, A.G. Livingston, *J. Membrane Sci.* **2018**, *558*, 52–63.

[26]   B. Satilmis, T. Uyar, *J. Coll. Interf. Sci.* **2018**, *516*, 317–324.

[27]   E. Madrid, P. Cottis, Y.Y. Rong, A.T. Rogers, J.M. Stone, R. Malpass-Evans, M. Carta, N.B. McKeown, F. Marken, *J. Mater. Chem. A*, **2015**, *3*, 15849–15853.

[28] B. Ghanem, F. Alghunaimi, N. Alaslai, X.H. Ma, I. Pinnau, *RSC Adv*. **2016**, *6*, 79625–79630.

[29] Z.X. Chen, P.P. Zou, R.Z. Zhang, L.Y. Dai, Y.Y. Wang, *Catal. Lett.* **2015**, *145*, 2029–2036.

[30] R.G. Compton, C.E. Banks, *Understanding Voltammetry*, World Scientific, London, 2007.

[31] F. Marken, J.D. Watkins, A.M. Collins, *Phys. Chem. Chem. Phys.* **2011**, *13*, 10036–10047.

[32] T. Grygar, F. Marken, U. Schröder, F. Scholz, *Coll. Czech. Chem. Commun.* **2002**, *67*, 163–208.

[33] T. Grygar, S. Kuckova, D. Hradil, J. Hradilova, *J. Solid State Electrochem*. **2003**, *7*, 706–713.

[34] G. Matricali, M.M. Dieng, J.F. Dufeu, M. Guillou, *Electrochim. Acta,* **1976**, *21*, 943–952.

[35] Y.Y. Rong, R. Malpass-Evans, M. Carta, N.B. McKeown, G.A. Attard, F. Marken, *Electrochem. Commun*. **2014**, *46*, 26–29.

[36] S.D. Ahn, A. Kolodziej, R. Malpass-Evans, M. Carta, N.B. McKeown, S.D. Bull, A. Buchard, F. Marken, *Electrocatalysis*, **2016**, *7*, 70–78.

[37] F. Scholz, *Electroanalytical Methods*, Springer, Berlin, 2010, p. 68.

[38] L.D. Burke, J.K. Casey, *J. Electrochem. Soc.* **1993**, *140*, 1284–1291.

[39] A.E. Bolzan, *J. Electroanal. Chem.* **1997**, *437*, 199–208.

[40] M.H. Seo, S.M. Choi, J.K. Seo, S.H. Noh, W.B. Kim, B. Han, *Appl. Catal. B Environm*. **2013**, *129*, 163–171.

[41] C.C. Hu, T.C. Wen, *J. Electrochem. Soc.* **1994**, *141*, 2996–3001.

[42] L.E.A. Berlouis, P.J. Hall, A.J. MacKinnon, A.W. Wark, D. Manuelli, V. Gervais, J.E. Robertson, *J. Alloys Compounds*, **1997**, *253*, 207–209.

[43] J.C. Calderon Gomez, R. Moliner, M. Jesus Lazaro, *Catalysts*, **2016**, *6*, 130.

[44] B.D. Adams, A.C. Chen, *Mater. Today*, **2011**, *14*, 282–289.

[45] M. Tian, B.E. Conway, *J. Electroanal. Chem.* **2005**, *581*, 176–189.

[46] S. Uhm, H.J. Lee, J. Lee, *Phys. Chem. Chem. Phys.* **2009**, *11*, 9326–9336.

[47] N.V. Rees, R.G. Compton, *J. Solid State Electrochem*. **2011**, *15*, 2095–2100.

[48] H. Meng, D.R. Zeng, F.Y. Xie, *Catalysts*, **2015**, *5*, 1221–1274.

[49] L. An, R. Chen, *J. Power Sources*, **2016**, *320*, 127–139.

[50] S.X. Leong, M. Carta, R. Malpass-Evans, N.B. McKeown, E. Madrid, F. Marken, *Electrochem. Commun*. **2018**, *86*, 17–20.

[51] X.T. Liu, P.H. Su, Y. Chen, B.L. Zhu, S.M. Zhang, W.P. Huang, *New J. Chem.* **2018**, *42*, 9449–9454.

[52] N.V. Long, C.M. Thi, Y. Yong, M. Nogami, M. Ohtaki, *J. Nanosci. Nanotechnol.* **2013**, *13*, 4799–4824.

[53] A. Mahajan, S. Banik, P.S. Roy, S.R. Chowdhury, S.K. Bhattacharya, *Int. J. Hydrogen Energy*, **2017**, *42*, 21263–21278.

[54] C. Bianchini, P.K. Shen, *Chem. Rev.* **2009**, *109*, 4183–4206.

[55] Q.F. Yi, Q.H. Chen, Z. Yang, *J. Power Sources*, **2015**, *298*, 171–176.

[56] C. Bianchini, P.K. Shen, *Chem. Rev.* **2009**, *109*, 4183–4206.

[57] M. Simoes, S. Baranton, C. Coutanceau, *ChemSusChem*, **2012**, *5*, 2106–2124.

[58] D.P. He, Y.Y. Rong, Z.K. Kou, S.C. Mu, T. Peng, R. Malpass-Evans, M. Carta, N.B. McKeown, F. Marken, *Electrochem. Commun*. **2015**, *59*, 72–76.